Published in final edited form as:
J Magn Reson. 2015 January ; 250: 45–54. doi:10.1016/j.jmr.2014.11.002.

Composite-180° Pulse-Based Symmetry Sequences to Recouple Proton Chemical Shift Anisotropy Tensors under Ultrafast MAS Solid-State NMR Spectroscopy

Manoj Kumar Pandey[1], **Michal Malon**[1,2], **Ayyalusamy Ramamoorthy**[3], and **Yusuke Nishiyama**[*,1,2]

[1]CLST NMR Facility, RIKEN, Yokohama, Kanagawa 230-0045, Japan

[2]JEOL RESONANCE Inc., Musashino, Akishima, Tokyo 196-8558, Japan

[3]Biophysics and Department of Chemistry, University of Michigan, Ann Arbor, MI 48109-1055, USA

Abstract

There is considerable interest in the measurement of proton (^{1}H) chemical shift anisotropy (CSA) tensors to obtain deeper insights into H-bonding interactions which find numerous applications in chemical and biological systems. However, the presence of strong ^{1}H/^{1}H dipolar interaction makes it difficult to determine small size ^{1}H CSAs from the homogeneously broadened NMR spectra. Previously reported pulse sequences for ^{1}H CSA recoupling are prone to the effects of radio frequency field (B_1) inhomogeneity. In the present work we have carried out a systematic study using both numerical and experimental approaches to evaluate γ-encoded radio frequency (RF) pulse sequences based on *R*-symmetries that recouple ^{1}H CSA in the indirect dimension of a 2D ^{1}H/^{1}H anisotropic/isotropic chemical shift correlation experiment under ultrafast magic angle spinning (MAS) frequencies. The spectral resolution and sensitivity can be significantly improved in both frequency dimensions of the 2D ^{1}H/^{1}H correlation spectrum without decoupling ^{1}H/^{1}H dipolar couplings but by using ultrafast MAS rates up to 70 kHz. We successfully demonstrate that with a reasonable RF field requirement (< 200 kHz) a set of symmetry-based recoupling sequences, with a series of phase-alternating $270°_0$-$90°_{180}$ composite-180° pulses, are more robust in combating B_1 inhomogeneity effects. In addition, our results show that the new pulse sequences render remarkable ^{1}H CSA recoupling efficiency and undistorted CSA lineshapes. Experimental results on citric acid and malonic acid comparing the efficiencies of these newly developed pulse

*Corresponding author yunishiy@jeol.co.jp.

Supporting Information Available

A table listing the calculated scaling factor ($|\kappa_{lm\lambda\mu}|$) for γ-encoded CSA recoupling symmetry-based sequences (RN_n^ν) and a figure comprised of recoupled ^{1}H CSA lineshapes from 2D ^{1}H/^{1}H anisotropic/isotropic chemical shift correlation experiments using $R18_8^7$ and $R20_9^8$ pulse sequences with a series of phase-alternating 180° pulses.

sequences with that of previously reported CSA recoupling pulse sequences are also reported under ultrafast MAS conditions.

Introduction

Due to limited spectroscopic resolution and sensitivity originating from strong anisotropic interactions in solids, atomic-level characterization using solid-state nuclear magnetic resonance (NMR) spectroscopy technique has always been a challenging task. Over the past several years, detection of low abundant nuclei (^{13}C, ^{15}N) has been a routinely employed method for solids due to their large spread of chemical shift frequency.[1,2] On the other hand, methods based on direct detection of protons are still emerging. The main difficulty associated with these methods is the homogeneously broadened ^{1}H resonances resulting from strong $^{1}H/^{1}H$ dipolar interactions due to their high abundance and sensitivity. However, sample spinning at ultrafast (up to 110 kHz) magic angle spinning (MAS) frequencies - in combination with the application of high magnetic field strength ($B_0 \geq 14.1$ T) can significantly improve the spectral resolution and sensitivity by completely suppressing the anisotropic interactions without any need for deuteration of the sample. This technique has opened up new avenues towards the development of proton detection-based experiments[3-8] on non-deuterated samples wherein full advantage of high sensitivity and natural abundance of protons can be taken into account. [9-15] While the isotropic chemical shift values allow us to distinguish magnetically inequivalent nuclear spins in the system, various anisotropic interactions contain unique information about its structure and dynamics. The information about the local electronic environment and motions surrounding a nucleus is provided by chemical shift anisotropy (CSA) tensors which play a significant role in detailed structural and dynamics investigations of an enormous number of chemical and biological systems by both solution and solid-state NMR spectroscopy.[16-20] A variety of recoupling techniques have been developed in the past to reintroduce CSA and dipolar couplings to measure structural constraints that are otherwise averaged out due to MAS.[21-27] Particularly, it is important to have the knowledge of proton CSA tensors to get greater insights into both inter and intra molecular H-bonding interactions which provide structural stability to biomolecules, polymers and molecular self-assemblies.[28-33] In this regard it is important to have accurately determined ^{1}H CSA tensors and understand their variation in detail for structural and dynamics studies. *Ab initio* quantum chemical calculation is generally performed for the better interpretation of H-bonding interactions on the basis of ^{1}H CSA.[34] Subsequent development of this approach has generated a huge interest amongst researchers to utilize ^{1}H CSA in order to get piercing insights into structures in a range of chemical and biological systems. Nevertheless, the size of ^{1}H CSA is relatively small and consequently its extraction from homogeneously broadened NMR spectra becomes difficult due to the presence of strong $^{1}H/^{1}H$ dipolar couplings. In recent years, there has been a gradual progress in the development of methods to determine ^{1}H CSA tensors from multidimensional experiments.[35-39] Most of these experiments necessitate a combination of MAS and homonuclear decoupling to get well resolved proton resonances for different proton sites in a solid sample. In a previous study, ^{1}H CSA was reintroduced using a symmetry-based recoupling sequence in the indirect dimension and the individual proton sites were well resolved at their respective isotropic chemical shift values using

homonuclear decoupling in the direct dimension of a 2D experiment.[35] However, the requirement of a strong RF field for homonuclear decoupling during acquisition and a relatively slow MAS for the symmetry sequence used in this study can be limiting factors of this approach. In another study, a 2D ^{1}H/^{1}H correlation experiment was performed at rotary resonance condition to reintroduce ^{1}H CSA in the indirect dimension in combination with fast MAS.[36] Again, this approach's extreme sensitivity to radio frequency field (B_1) inhomogeneity can constrain the accurate determination of ^{1}H CSA tensors. In a recent report, CSA tensors for amide protons of U-^{13}C, ^{15}N-CAP-Gly domain of dynactin were determined by implementing symmetry-based sequence in 3D experiments wherein ^{1}H CSA was first recoupled in the indirect dimension with a subsequent magnetization transfer to a directly bonded heteronucleus.[37,38] In another study, ^{1}H CSA tensors for OH hydrogen-bonded protons in tyrosine.HCl and citric acid were determined using symmetry-based recoupling sequence $R16_3^2$.[39] Therein, 2D ^{1}H anisotropic-isotropic chemical shift correlation experiments were performed in combination with ultrafast MAS and high B_0 field, and without the application of homonuclear decoupling. Nevertheless, the existing symmetry-based ^{1}H CSA recoupling sequences are sensitive to RF field (B_1) inhomogeneity, resulting in lineshape distortion, poor signal-to-noise ratio (SNR) due to a strong center peak arising from non-oscillating components, and poor resolution and sensitivity. To overcome these difficulties, we have systematically carried out a study to find a set of more efficient symmetry-based CSA recoupling sequences as compared to earlier reported sequences based on *R*-symmetries through extensive numerical simulations in combination with experiments. Herein, we demonstrate that symmetry-based 2D ^{1}H CSA recoupling sequences with a series of phase-alternating $270°_0$-$90°_{180}$ composite-180° pulses are more robust towards the presence of RF field (B_1) inhomogeneity as compared to the previously reported symmetry-based sequence with a series of phase-alternating 180° pulses under ultrafast MAS condition and high B_0 strength. The spectral resolution and sensitivity can be significantly improved both in the direct (isotropic chemical shift) and indirect (CSA) dimensions of a 2D ^{1}H/^{1}H correlation spectrum without the application of ^{1}H/^{1}H dipolar decoupling under ultrafast MAS rates. The use of ultrafast MAS rates (≥ 60 kHz), largely removes strong ^{1}H/^{1}H dipolar interactions, and high B_0 field strength (16.4 Tesla) is used to amplify small sized ^{1}H CSAs. We demonstrate the robustness of the new CSA recoupling sequences over the existing methods on powder samples of citric acid and malonic acid.

Selection of CSA recoupling pulse sequences

We have implemented γ-encoded rotor-synchronized pulse sequences of symmetry class RN_n^ν to recouple ^{1}H CSA through the first order average Hamiltonian as described in detail by Levitt and co-workers.[40-42] *N*,*n* and ν are integers and represent symmetry numbers associated with rotor-synchronized pulses wherein each rotational period $n\tau_r$ (τ_r: cycle time of sample spinning) is subdivided into *N* phase alternated inversion pulse elements such that each pulse has a length of $n\tau_r/N$ and a phase of $\pm \pi\nu/N$. To begin with we performed a systematic selection of pulse sequences suitable for the present study from a list of possible γ-encoded symmetry-based sequences RN_n^ν, given elsewhere.[40] The basic criteria for the selection of symmetry-based CSA recoupling pulse sequences suitable for the experimental data collection is fivefold: 1) ^{1}H CSA is recoupled through the first-order average

Hamiltonian, 2) recoupling of $^{1}H/^{1}H$ dipolar interactions along with ^{1}H isotropic chemical shifts are avoided, 3) RF field amplitude, which is proportional to the MAS rate in symmetry-based sequence, is kept below 200 kHz at a MAS rate of 70 kHz to avoid any damage to the NMR probe, 4) a large scaling factor is desired as the span of ^{1}H CSA is small, and 5) the effect of RF field inhomogeneity is minimized.

The first two criteria are satisfied by a selection of $\{l, m, \lambda, \mu\}$ equal to $\{2, \pm2, 1, \pm1\}$ or $\{2, \pm2, 1, \mp 1\}$ terms where l and λ are space and spin rank with components m and μ, respectively. All inequivalent solutions for symmetry-based sequences RN_n^ν in the range $N \leq 20$, $n \leq 10$ and $\nu \leq 10$ can be found elsewhere.[40] Besides the choice of the symmetry numbers, the inversion pulse elements used in the symmetry-based sequences can significantly affect their practical performance. Consequently, in this study, we have implemented two different pulse sequences; a) a series of phase-alternating 180° pulses, and b) a series of phase-alternating $270°_0$-$90°_{180}$ composite-180° pulses. It is to be noted that both CSA and heteronuclear dipolar interactions have the same symmetry with respect to sample and spin rotations; therefore ^{1}H CSA recoupling sequences simultaneously recouple heteronuclear (^{1}H-X) dipolar interactions as well. Nevertheless, heteronuclear dipolar interactions can be decoupled by applying a 180° pulse on the X-channel in the middle of the CSA recoupling pulses.[37] Since the X nuclei (or $^{13}C/^{15}N$) are not abundant in the systems investigated in this study, all the experiments were carried without any application of 180° pulse on the X-channel. Out of 32 γ-encoded CSA recoupling symmetry sequences listed elsewhere,[40] we selected 24 sequences composed of a series of phase-alternating 180° pulses to satisfy the third criteria wherein the RF amplitude requirement was well within the limit under ultrafast MAS rates (in the range 60-70 kHz) (Figure 1A1). Obviously, the RF amplitude for the sequence with a series of phase-alternating $270°_0$-$90°_{180}$ composite-180° pulses is two times higher than the RF amplitude associated with 180° pulses. This rules out some of the sequences and the number of symmetry sequences for this class reduces to 18 (Figure 1A2). To meet the fourth criteria we calculated scaling factor ($\kappa_{lm\lambda\mu}$) for these sequences (refer to Supporting Information for the values of scaling factor) and selected sequences with $|\kappa_{lm\lambda\mu}| \geq 0.13$. The γ-encoded recoupling sequences result in amplitude modulated signal intensity which requires an application of real Fourier transform of FID; consequently, the sign of CSA cannot be determined. On the basis of the value of scaling factor, we chose symmetry sequences $R14_3^1$, $R16_3^2$, $R14_4^1$, $R18_4^1$ and $R18_5^1$ with a series of phase-alternating 180° pulses (Figure 1B1), and $R12_5^4$, $R14_5^3$, $R14_6^5$, $R16_7^6$, $R18_7^5$, $R20_7^4$, $R14_8^5$, $R18_8^7$, $R16_9^6$, $R20_9^8$ and $R18_{10}^7$ with a series of phase-alternating $270°_0$-$90°_{180}$ composite-180° pulses (Figure 1B2). To select the sequences which are robust towards RF field inhomogeneity so as to fulfill the fifth criteria we carried out numerical simulations using SIMPSON[43,44] both in the absence and presence of RF field inhomogeneity (Figure 2) implementing ^{1}H CSA recoupling sequences with the scaling factor $|\kappa_{lm\lambda\mu}| \geq 0.13$. We assumed a Gaussian shaped distribution of the RF field strengths centered at a nominal RF field strength with a standard deviation of 0.1. The presence of RF field inhomogeneity resulted in the center peak with varying intensity from these symmetry-based sequences in contrast to those observed in the absence of RF field inhomogeneity. Spectra obtained with many of these recoupling sequences exhibited a strong center peak, and hence a strong

dependence on RF field inhomogeneity. It is essential to point out here that the presence of a strong center peak results in low SNR and hence poor resolution and sensitivity, and significant distortions in the recoupled powder lineshapes. To remove this center peak, DC balance (accomplished by subtracting the average of the final 1/8th points in t_1 from total data points) is often applied prior to a real Fourier transform, but only at the cost of sensitivity of CSA powder lineshape which in turn makes it difficult to observe smaller CSAs due to their interference resulting from the strong center peak. All the symmetry-sequences with a series of phase-alternating 180° pulses and $|\kappa_{lm\lambda\mu}| \geq 0.13$ were found to have strong dependence on RF field inhomogeneity leading to high center peak intensities with a distinct change in CSA lineshapes along with recoupling efficiencies in comparison to that observed in the absence of RF field inhomogeneity. Consequently, these sequences might lead to inaccurate ^{1}H CSA parameters and hence can be ruled out (Figure 1C1). On the other hand, except minor variations in center peak intensities, recoupled powder lineshapes as well as recoupling efficiency obtained from most of the above listed symmetry sequences with a series of 270°$_0$-90°$_{180}$ composite-180° pulses and $|\kappa_{lm\lambda\mu}| \geq 0.13$ remained nearly unperturbed both in the presence and absence of RF field inhomogeneity and explain their robustness towards RF field inhomogeneity. On the basis of low center peak intensity we finally concluded that symmetry-based sequences $R12_5^4$, $R14_6^5$, $R16_7^6$, $R14_8^5$, $R18_8^7$, $R16_9^6$, $R20_9^8$ and $R18_{10}^7$ with a series of phase-alternating 270°$_0$-90°$_{180}$ composite-180° pulses (Figure 1C2) are the best set of sequences that can be implemented to extract ^{1}H CSAs under ultrafast MAS conditions. Out of the eight symmetry-based sequences mentioned above, $R16_7^6$, $R18_8^7$ and $R20_9^8$ are found to be almost identical in terms of CSA recoupling efficiency, scaling factor and center peak intensity while $R12_5^4$ and $R14_6^5$ resulted in a slightly higher center peak intensity and $R14_8^5$, $R16_9^6$ and $R18_{10}^7$ have relatively smaller scaling factor as compared to the other three sequences. It is worth mentioning that most of the γ-encoded symmetry-based sequences with the ratio of symmetry numbers $N/2n < 2$ shown in the present study are robust in combating the presence of RF field inhomogeneity. Nevertheless, there may be a few exceptions to this, as seen from Figure 2, wherein the ^{1}H CSA lineshape using symmetry-based sequence $R18_5^1\ (N/2n<2)$, with a series of phase-alternating 180° pulses, has a strong dependence on RF field inhomogeneity. To further substantiate the right selection of ^{1}H CSA recoupling sequences that are robust towards RF field inhomogeneity, we carried out numerical simulations by deliberately mis-setting the RF amplitudes of recoupling pulses from the theoretical value. It is evident from Figure 3 that mismatches of the RF amplitude by ±10% lead to strong center peaks as well as huge distortions in the CSA lineshapes when $R16_3^2\ (180^\circ)$ is used, unlike $R18_8^7\ (270^\circ 90^\circ)$ wherein an undistorted CSA lineshapes with relatively weak center peaks are observed. This observation clearly rationalizes our approach for the selection of robust ^{1}H CSA recoupling sequences towards RF field inhomogeneity on the basis of the center peak intensity. For a demonstration purpose in this study we have carried out experimental measurements using symmetry sequences $R16_3^2$ with a series of phase-alternating 180° pulses, and $R18_8^7$ and $R20_9^8$ with a series of phase-alternating 270°$_0$-90°$_{180}$ composite-180° pulses. Hereafter we will be using the notations $R16_3^2\ (180^\circ)$, $R18_8^7\ (270^\circ 90^\circ)$ and $R20_9^8\ (270^\circ 90^\circ)$ to represent the symmetry-based sequences, $R16_3^2$, $R18_8^7$ and $R20_9^8$, respectively.

Experimental

All NMR experiments were performed on a 700 MHz solid-state NMR spectrometer (JEOL ECA700II) using a 1.0 mm double-resonance ultrafast MAS probe (JEOL RESONANCE Inc.) at spinning frequencies up to 70 kHz. One mg of citric acid or malonic acid was packed in a 1 mm zirconia rotor and all measurements were carried out at room temperature (~23°C). Two dimensional (2D) symmetry-based pulse sequences $R16_3^2\,(180^\circ)$, $R18_8^7\,(270^\circ 90^\circ)$ and $R20_9^8\,(270^\circ 90^\circ)$ used in this study to record proton-detected 2D ^{1}H/^{1}H anisotropic/isotropic chemical shift correlation spectra under ultrafast MAS frequencies are shown in Figure 4. Each *R* block in $R16_3^2\,(180^\circ)$ pulse sequence is composed of a 180° pulse whereas $R18_8^7\,(270^\circ 90^\circ)$ and $R20_9^8\,(270^\circ 90^\circ)$ are composed of 270° and 90° pulses. Table 1 gives the list of all parameters associated with symmetry-based sequences used in this study. All NMR data were acquired using an acquisition time of 10.24 ms with 1024 t_2 complex points. The amplitude modulated t_1 signal with 32 points and 3 scans per t_1 points was obtained at every $N\tau_r$ for $R18_8^7\,(270^\circ 90^\circ)$ and $R20_9^8\,(270^\circ 90^\circ)$ and every $3N\tau_r$ for $R16_3^2\,(180^\circ)$ to keep the spectral width in the indirect dimension at par with each other. A relaxation delay of 120 s was set prior to the application of symmetry-based recoupling pulses. All spectra were processed using Delta NMR software (JEOL RESONANCE Inc.). While the t_1 domain was Fourier transformed after zero filling, DC balance followed by zero filling was applied prior to real Fourier transformation in the t_2 domain. The isotropic and anisotropic chemical shifts, and the asymmetry parameter are defined as $\delta_{iso} = (\delta_{xx}+\delta_{yy}+\delta_{zz})/3$, $\delta_{ani} = |\delta_{zz}-\delta_{iso}|$, and $\eta = (\delta_{yy}-\delta_{xx})/\delta_{ani}$, respectively, wherein δ_{xx}, δ_{yy} and δ_{zz} are the principal components of chemical shift tensor such that $|\delta_{zz}-\delta_{iso}| \geq |\delta_{xx}-\delta_{iso}| \geq |\delta_{yy}-\delta_{iso}|$.

Results and discussion

In this section the performances of a previously reported ^{1}H CSA recoupling symmetry sequence $R16_3^2\,(180^\circ)$ and the new sequences $R18_8^7\,(270^\circ 90^\circ)$ and $R20_9^8\,(270^\circ 90^\circ)$ developed in this study are examined by carrying out 2D ^{1}H/^{1}H anisotropic/isotropic chemical shift correlation experiments under ultrafast MAS conditions on citric acid and malonic acid. A discussion on these results will be followed by demonstration of the role of ultrafast MAS to suppress strong ^{1}H/^{1}H homonuclear dipolar interactions to get undistorted recoupled ^{1}H CSA lineshapes.

^{1}H CSA recoupling experiments on citric acid and malonic acid

On the basis of results obtained from numerical simulations, we carried out ^{1}H CSA recoupling experiments using symmetry-based sequences $R16_3^2\,(180^\circ)$, $R18_8^7\,(270^\circ 90^\circ)$ and $R20_9^8\,(270^\circ 90^\circ)$ on citric acid and malonic acid at ultrafast MAS rates of 70 and 60 kHz, respectively. 2D anisotropic/isotropic chemical shift correlation spectra recorded using the symmetry-based sequences described above are shown in Figure 5 (A) and (C) for citric acid and malonic acid, respectively. The ultrafast MAS spectra show well-resolved peaks both for citric acid and malonic acid in the isotropic dimension without application of ^{1}H/^{1}H homonuclear decoupling. It is worthwhile to mention here that narrow center peaks with

high intensity were regularly observed from our experiments. Consequently, ^{1}H CSA lineshapes were largely affected by the wiggles/oscillations from these center peaks which affect the extraction of ^{1}H CSA. As suggested in earlier reports,[37,39] the origin of these center peaks is due to certain non-ideal conditions and one of them is believed to be the presence of RF field inhomogeneity. These conditions result in a slow decay and/or no decay of some longitudinal magnetization that leads to a DC offset in the time domain and hence the center peak in the indirect frequency dimension. As pointed out earlier, a DC balance was applied prior to the real Fourier transform in the indirect dimension to reduce the DC offset resulting from undecayed longitudinal magnetization. A comparison of ^{1}H CSA recoupling efficiency obtained from the spectral slices at isotropic ^{1}H chemical shifts using symmetry-based sequences $R16_3^2\,(180^\circ)$, $R18_8^7\,(270^\circ 90^\circ)$ and $R20_9^8\,(270^\circ 90^\circ)$ in the direct dimension are shown in Figure 5 (B) and (D), respectively. It is obvious from the spectral slices obtained from 2D spectra that the sensitivity of recoupled ^{1}H CSA lineshapes can be significantly improved by implementing symmetry-based recoupling sequences $R18_8^7\,(270^\circ 90^\circ)$ and $R20_9^8\,(270^\circ 90^\circ)$ in comparison to the reported symmetry-based sequence $R16_3^2\,(180^\circ)$ under the ultrafast MAS condition. This observation is completely in accordance with our results based on numerical simulations as described earlier. Furthermore, significant distortions in ^{1}H CSA lineshapes could also be seen using a symmetry-based sequence $R16_3^2\,(180^\circ)$ which might lead to an error in the ^{1}H CSA values. It is noteworthy that in the case of malonic acid the effect of RF field inhomogeneity on the center peaks is more significant as compared to citric acid (Figure 5 (D)). This could probably be due to the slow MAS rate (60 kHz) used for 2D data collection and this effect can be minimized at MAS rates ≥ 70 kHz.

Numerical simulations using SIMPSON were performed to extract ^{1}H CSA and asymmetry parameter values by fitting the experimental ^{1}H CSA lineshapes using symmetry-based pulse sequences $R16_3^2\,(180^\circ)$, $R18_8^7\,(270^\circ 90^\circ)$ and $R20_9^8\,(270^\circ 90^\circ)$ for test samples citric acid and malonic acid as shown in Figure 6. All the simulations were carried out by taking a single spin system representative of a single quantum first-order average Hamiltonian using 678 (α, β) orientations and 26 γ angles for powder averaging at 700 MHz ^{1}H Larmor frequency in the absence of RF field inhomogeneity. The vertical scaling and line broadening of simulated ^{1}H CSA lineshapes were adjusted to fit the experimental lineshapes. The best fit parameters are listed in Table 2. ^{1}H CSA values obtained from the best fit from all the three recoupling experiments are generally in good agreement with earlier reported values both under ultrafast MAS[39] and slow MAS[35] rates for citric acid. Additionally, certain deviations from numerical simulations are observed in the zero-frequency region of the spectrum resulting mainly from RF field inhomogeneity that can contribute to the uncertainty in the determination of asymmetry parameter. While, we believe that the main contribution to center peak is from the presence of RF field inhomogeneity, other sources such as the amplitude and/or phase transient effects, and the deviation in rotor phase due to fluctuations in sample spinning may also contribute to the observed discrepancy. As pointed out earlier, $R16_3^2$ gives distorted CSA lineshapes both for small and large ^{1}H CSAs and can lead to errors in the extraction of CSA values from the data fitting. In particular, in the case where CSA is small, the symmetry sequence

$R16_3^2(180^\circ)$ leads to ^{1}H CSA lineshapes that differ significantly from the lineshapes obtained from symmetry sequences $R18_8^7(270^\circ 90^\circ)$ and $R20_9^8(270^\circ 90^\circ)$. This phenomenon can be attributed to the strong dependence of recoupling efficiency on RF field inhomogeneity for the symmetry sequence $R16_3^2(180^\circ)$ which results in significant contribution to recoupled powder lineshapes for a small CSA while this imperfection is slightly reduced for a large CSA. There is a possibility that first-order single-quantum average Hamiltonian comprised of a single spin might not be sufficient to explain the spin dynamics in the case of symmetry sequence $R16_3^2$ and may require corrections to higher-order terms in the Hamiltonian to get the best fit. In contrast to this, CSA lineshapes using sequences $R18_8^7(270^\circ 90^\circ)$ and $R20_9^8(270^\circ 90^\circ)$ fit extremely well with the calculated lineshapes both for small as well as large CSAs and validates the robustness towards the presence of RF field inhomogeneity. We would like to mention here that the γ-encoded symmetry-based sequences, for e.g., $R18_8^7$ and $R20_9^8$ with a series of phase-alternating 180° pulses, can also be used for recoupling of ^{1}H CSAs at ultrafast MAS; however there can be certain limitations in implementing these sequences because of the small scaling factor (refer to Table S1 of Supporting Information for the values) and their behavior towards the presence of RF field inhomogeneity. It can be seen from Figure S1 of Supporting Information that the center frequency region of experimental ^{1}H CSA lineshape is affected most probably by the presence of RF field inhomogeneity for all ^{1}H resonances of citric acid, in contrast to ^{1}H CSA lineshapes obtained using the same symmetry-based sequences but with phase-alternating 270°_0-90°_{180} composite-180° pulses (Figures 5 or 6). This effect is significant especially when recoupling small size CSAs - an observation which is similar to that for the use of $R16_3^2(180^\circ)$.

Suppression of strong ^{1}H/^{1}H homonuclear dipolar interactions using Ultrafast MAS

In this section we demonstrate the importance of ultrafast MAS to get undistorted ^{1}H CSA lineshapes using symmetry-based sequence. The γ-encoded CSA recoupling symmetry-sequences based on *R*-symmetries suppress isotropic chemical shift and homonuclear dipolar interaction resulting in the first-order average Hamiltonian comprised of a single spin. The use of moderate MAS rates (30-40 kHz) may not be sufficient to suppress ^{1}H/^{1}H dipolar interactions completely for strongly coupled systems. This can lead to distorted ^{1}H CSA lineshapes resulting from the second-order effects due to unsuppressed anisotropic interactions. Alternatively, the role of ultrafast MAS becomes important to suppress ^{1}H/^{1}H dipolar interactions completely in the strongly coupled spin systems. In order to show the necessity of ultrafast MAS so as to get undistorted CSA lineshapes originating from the second-order effects due to insufficient suppression of strong ^{1}H/^{1}H dipolar interactions we carried out numerical simulations on a five spin network representative of a $-CH_2-CH-CH_2-$ system by changing MAS rates. All the simulations were performed using symmetry-based sequence $R18_8^7(270^\circ 90^\circ)$ at MAS rates of 40, 60, 80 and 100 kHz. As shown earlier, this pulse sequence is more robust towards the presence of RF field inhomogeneity and leads to almost similar lineshape both in the absence and presence of RF filed inhomogeneity; therefore we avoided the inclusion of RF field inhomogeneity in simulations to reduce the simulation time. In the simulations CSA recoupling efficiency was

calculated for −CH− proton which is surrounded by four strongly coupled $-CH_2$ protons and the initial density operator was taken as a sum of initial z-magnetization associated with each spin. As seen from Figure 7, distortion in the recoupled CSA lineshape is observed at a slow MAS rate of 40 kHz due to the presence of unsuppressed $^1H/^1H$ dipolar interactions. Moreover, these distortions could be significant for sequences like $R16_3^2\,(180^\circ)$ and $R14_3^1\,(180^\circ)$, which are more sensitive towards the presence of RF field inhomogeneity and can lead to error in the measurements of CSA parameters. Nevertheless, these distortions in the CSA lineshape can well be removed by spinning the sample at MAS rates greater than or equal to 60 kHz which results in a better suppression of $^1H/^1H$ dipolar interactions also seen from Figure 7. Furthermore, the choice of MAS rates can vary depending on the type of recoupling sequence used. As seen from Figure 7, a reduction in the center peak intensity with the increase in the spinning rate is observed which clearly recommends experiments to be performed under ultrafast MAS to minimize the contribution from multi-spins so as to suppress the center peak. Above all, the efficiency of the recoupled CSA lineshape can be improved under ultrafast MAS condition which is of huge importance for the case of CSA recoupling sequences with poor SNR. These observations obviously necessitate the use of ultrafast MAS to carryout ^1H CSA measurements. Moreover, ultrafast MAS provides wider spectral width $1 / n\tau_r$ that allows the use of symmetry-based sequences with a large symmetry number *n*.

Conclusions

In this study, we have reported a systematic selection of γ-encoded symmetry-based sequences based on *R*-symmetries suitable for ^1H CSA recoupling under ultrafast MAS condition on the basis of symmetry numbers, RF field requirement, scaling factor and robustness towards RF field inhomogeneity using numerical simulations. We have shown that a set of γ-encoded symmetry-based sequences, with a series of phase-alternating $270°_0$-$90°_{180}$ composite-180° pulses are found to be more robust towards the presence of RF field inhomogeneity in comparison to earlier reported sequences with a series of phase-alternating 180° pulses under ultrafast MAS condition. Our results from numerical simulations are cross-validated through 2D $^1H/^1H$ anisotropic/isotropic chemical shift correlation experiments carried out under ultrafast MAS conditions on citric acid and malonic acid. We have demonstrated that the previously reported ^1H CSA recoupling symmetry sequence $R16_3^2\,(180^\circ)$, is extremely sensitive to RF field inhomogeneity that severely distorts the observed ^1H CSA lineshapes and significantly reduces the sensitivity. On the other hand the new sequences proposed in this study, $R18_8^7\,(270^\circ 90^\circ)$ and $R20_9^8\,(270^\circ 90^\circ)$ successfully suppress RF field inhomogeneity effects and result in undistorted recoupled ^1H CSA lineshapes with significantly improved sensitivity. We have determined ^1H CSA parameters by fitting the recoupled CSA lineshapes obtained from experiments for malonic acid and citric acid using numerical simulations. The recoupled ^1H CSA lineshapes correlate well with calculated lineshapes obtained from the first-order average Hamiltonian. Furthermore, we have also discussed the role of ultrafast MAS for better suppression of strong $^1H/^1H$ dipolar interactions through numerical simulations. We believe that the proposed symmetry-based recoupling pulse sequences in this study can be

easily implemented in multidimensional ^{1}H CSA recoupling experiments under ultrafast MAS conditions both in the presence and absence of heteronuclei which will be a step forward to get better insights into the studies relying on ^{1}H CSA tensors.

Supplementary Material

Refer to Web version on PubMed Central for supplementary material.

Acknowledgments

This research was supported by funds from JEOL RESONANCE Inc. (Tokyo, Japan) and NIH (GM084018 and GM095640 to A.R.). We would like to thank the JEOL RESONANCE scientists for help with spectrometer and ultrafast MAS probe.

References

1. Abragam, A. The Principles of Nuclear Magnetism. Clarendon Press; Oxford, England: 1961.
2. Mehring, M. Principles of High Resolution NMR in Solids. Springer-Verlag; Berlin: 1983.
3. Asami S, Reif B. Proton-Detected Solid-State NMR Spectroscopy at Aliphatic Sites: Application to Crystalline Systems. Acc Chem Res. 2013; 46:2089–2097. [PubMed: 23745638]
4. Asami S, Rakwalska-Bange M, Carlomagno T, Reif B. Protein-RNA Interfaces Probed by ^{1}H-Detected Mas Solid-State NMR Spectroscopy. Angew Chem. 2013; 52:2345–2349. [PubMed: 23335059]
5. Knight MJ, Felli IC, Pierattelli R, Bertini I, Emsley L, Herrmann T, Pintacuda G. Rapid Measurement of Pseudocontact Shifts in Metalloproteins by Proton-Detected Solid-State NMR Spectroscopy. J Am Chem Soc. 2012; 134:14730–14733. [PubMed: 22916960]
6. Huber M, Hiller S, Schanda P, Ernst M, Bockmann A, Verel R, Meier BH. A Proton-Detected 4D Solid-State NMR Experiment for Protein Structure Determination. Chem Phys Chem. 2011; 12:915–918. [PubMed: 21442705]
7. Huber M, Bockmann A, Hiller S, Meier BH. 4dD Solid-State NMR for Protein Structure Determination. Phys Chem Chem Phy. 2012; 14:5239–5246.
8. Nishiyama Y, Malon M, Ishii Y, Ramamoorthy A. 3D ^{15}N/^{15}N/^{1}H Chemical Shift Correlation Experiment Utilizing an Rfdr-Based ^{1}H/^{1}H Mixing Period at 100 KHz MAS. J Magn Reson. 2014; 244:1–5. [PubMed: 24801998]
9. Kobayashi T, Mao K, Paluch P, Nowak-Krol A, Sniechowska J, Nishiyama Y, Gryko DT, Potrzebowski MJ, Pruski M. Study of Intermolecular Interactions in the Corrole Matrix by Solid-State NMR under 100 KHz MAS and Theoretical Calculations. Angew Chem. 2013; 52:14108–14111. [PubMed: 24227750]
10. Ye YQ, Malon M, Martineau C, Taulelle F, Nishiyama Y. Rapid Measurement of Multidimensional ^{1}H Solid-State NMR Spectra at Ultra-Fast MAS Frequencies. J Magn Reson. 2014; 239:75–80. [PubMed: 24424008]
11. Deschamps M. Ultra-Fast MAS NMR Studies. Ann Rep NMR Spec. 2014; 81:109–144.
12. Samoson A, Tuherm T, Past J, Reinhold A, Anupold T, Heinmaa I. New Horizons for Magic-Angle Spinning NMR. Topics in Curr Chem. 2005; 246:15–31.
13. Nishiyama Y, Malon M, Gan Z, Endo Y, Nemoto T. Proton-Nitrogen-14 Overtone Two-Dimensional Correlation NMR Spectroscopy of Solid-Sample at Very Fast Magic Angle Sample Spinning. J Magn Reson. 2013; 230:160–164. [PubMed: 23542742]
14. Zhou DH, Shah G, Cormos M, Mullen C, Sandoz D, Rienstra CM. Proton-Detected Solid-State NMR Spectroscopy of Fully Protonated Proteins at 40 KHz Magic-Angle Spinning. J Am Chem Soc. 2007; 129:11791–11801. [PubMed: 17725352]
15. Marchetti A, Jehle S, Felletti M, Knight MJ, Wang Y, Xu ZQ, Park AY, Otting G, Lesage A, Emsley L, Dixon NE, Pintacuda G. Backbone Assignment of Fully Protonated Solid Proteins by

1h Detection and Ultrafast Magic-Angle-Spinning NMR Spectroscopy. Angew Chem. 2012; 51:10756–10759. [PubMed: 23023570]

16. Saito H, Ando I, Ramamoorthy A. Chemical Shift Tensor - the Heart of NMR: Insights into Biological Aspects of Proteins. Prog Nucl Mag Res Spec. 2010; 57:181–228. and references therein.
17. Oldfield E. Chemical Shifts in Amino Acids, Peptides, and Proteins: From Quantum Chemistry to Drug Design. Ann Rev Phys Chem. 2002; 53:349–378. [PubMed: 11972012]
18. Pandey MK, Vivekanandan S, Ahuja S, Pichumani K, Im SC, Waskell L, Ramamoorthy A. Determination of ^{15}N Chemical Shift Anisotropy from a Membrane-Bound Protein by NMR Spectroscopy. J Phys Chem B. 2012; 116:7181–7189. [PubMed: 22620865]
19. Pandey MK, Vivekanandan S, Ahuja S, Huang R, Im SC, Waskell L, Ramamoorthy A. Cytochrome-P450-Cytochrome-b_5 Interaction in a Membrane Environment Changes ^{15}N Chemical Shift Anisotropy Tensors. J Phys Chem B. 2013; 117:13851–13860. [PubMed: 24107224]
20. Laws DD, Bitter HM, Jerschow A. Solid-State NMR Spectroscopic Methods in Chemistry. Ange Chem. 2002; 41:3096–3129.
21. De Paepe G. Dipolar Recoupling in Magic Angle Spinning Solid-State Nuclear Magnetic Resonance. Ann Rev Phys Chem. 2012; 63:661–684. [PubMed: 22404583]
22. Hou GJ, Byeon IJL, Ahn J, Gronenborn AM, Polenova T. Recoupling of Chemical Shift Anisotropy by R-Symmetry Sequences in Magic Angle Spinning NMR Spectroscopy. J Chem Phys. 2012; 137:134201. [PubMed: 23039592]
23. Tycko R, Dabbagh G, Mirau PA. Determination of Chemical-Shift-Anisotropy Lineshapes in a Two-Dimensional Magic-Angle-Spinning NMR Experiment. J Magn Reson. 1989; 85:265–274.
24. Liu SF, Mao JD, Schmidt-Rohr K. A Robust Technique for Two-Dimensional Separation of Undistorted Chemical-Shift Anisotropy Powder Patterns in Magic-Angle-Spinning NMR. J Magn Reson. 2002; 155:15–28. [PubMed: 11945029]
25. Chan JCC, Tycko R. Recoupling of Chemical Shift Anisotropies in Solid-State NMR under High-Speed Magic-Angle Spinning and in Uniformly ^{13}C-Labeled Systems. J Chem Phys. 2003; 118:8378–8389.
26. Wylie BJ, Franks WT, Graesser DT, Rienstra CM. Site-Specific 13c Chemical Shift Anisotropy Measurements in a Uniformly ^{15}N,^{13}C-Labeled Microcrystalline Protein by 3D Magic-Angle Spinning NMR Spectroscopy. J Am Chem Soc. 2005; 127:11946–11947. [PubMed: 16117526]
27. Huang KY, Siemer AB, McDermott AE. Homonuclear Mixing Sequences for Perdeuterated Proteins. J Magn Reson. 2011; 208:122–127. [PubMed: 21094063]
28. Berglund B, Vaughan RW. Correlations between Proton Chemical-Shift Tensors, Deuterium Quadrupole Couplings, and Bond Distances for Hydrogen-Bonds in Solids. J Chem Phys. 1980; 73:2037–2043.
29. Tjandra N, Bax A. Solution NMR Measurement of Amide Proton Chemical Shift Anisotropy in ^{15}N-Enriched Proteins. Correlation with Hydrogen Bond Length. J Am Chem Soc. 1997; 119:8076–8082.
30. Loth K, Pelupessy P, Bodenhausen G. Chemical Shift Anisotropy Tensors of Carbonyl, Nitrogen, and Amide Proton Nuclei in Proteins through Cross-Correlated Relaxation in NMR Spectroscopy. J Am Chem Soc. 2005; 127:6062–6068. [PubMed: 15839707]
31. Yao LS, Grishaev A, Cornilescu G, Bax A. The Impact of Hydrogen Bonding on Amide ^{1}H Chemical Shift Anisotropy Studied by Cross-Correlated Relaxation and Liquid Crystal NMR Spectroscopy. J Am Chem Soc. 2010; 132:10866–10875. [PubMed: 20681720]
32. Gerald R, Bernhard T, Haeberlen U, Rendell J, Opella S. Chemical-Shift and Electric-Field Gradient Tensors for the Amide and Carboxyl Hydrogens in the Model Peptide N-Acetyl-D,L-Valine - Single-Crystal Deuterium NMR-Study. J Am Chem Soc. 1993; 115:777–782.
33. Wei YF, Lee DK, Hallock KJ, Ramamoorthy A. One-Dimensional ^{1}H-Detected Solid-State NMR Experiment to Determine Amide-^{1}H Chemical Shifts in Peptides. Chem Phys Lett. 2002; 351:42–46.
34. Charpentier T. The Paw/Gipaw Approach for Computing NMR Parameters: A New Dimension Added to NMR Study of Solids. Solid State Nucl Magn. 2011; 40:1–20.

35. Brouwer DH, Ripmeester JA. Symmetry-Based Recoupling of Proton Chemical Shift Anisotropies in Ultrahigh-Field Solid-State NMR. J Magn Reson. 2007; 185:173–178. [PubMed: 17188919]

36. Duma L, Abergel D, Tekely P, Bodenhausen G. Proton Chemical Shift Anisotropy Measurements of Hydrogen-Bonded Functional Groups by Fast Magic-Angle Spinning Solid-State NMR Spectroscopy. Chem Comm. 2008:2361–2363. [PubMed: 18473070]

37. Hou GJ, Paramasivam S, Yan S, Polenova T, Vega AJ. Multidimensional Magic Angle Spinning NMR Spectroscopy for Site-Resolved Measurement of Proton Chemical Shift Anisotropy in Biological Solids. J Am Chem Soc. 2013; 135:1358–1368. [PubMed: 23286322]

38. Hou GJ, Gupta R, Polenova T, Vega AJ. A Magic-Angle-Spinning NMR Spectroscopy Method for the Site-Specific Measurement of Proton Chemical-Shift Anisotropy in Biological and Organic Solids. Isr J Chem. 2014; 54:171–183. [PubMed: 25484446]

39. Miah HK, Bennett DA, Iuga D, Titman JJ. Measuring Proton Shift Tensors with Ultrafast MAS NMR. J Magn Reson. 2013; 235:1–5. [PubMed: 23911900]

40. Levitt, M. Symmetry-Based Pulse Sequences in Magic-Angle Spinning Solid-State NMR. In: Grant, DM.; Harris, RK., editors. Encycl Nuc Magn Reson. Vol. 9. Wiley; Chichester: 2002. p. 165-196.

41. Brinkmann A, Levitt MH. Symmetry Principles in the Nuclear Magnetic Resonance of Spinning Solids: Heteronuclear Recoupling by Generalized Hartmann-Hahn Sequences. J Chem Phys. 2001; 115:357–384.

42. Eden M, Levitt MH. Pulse Sequence Symmetries in the Nuclear Magnetic Resonance of Spinning Solids: Application to Heteronuclear Decoupling. J Chem Phys. 1999; 111:1511–1519.

43. Bak M, Rasmussen JT, Nielsen NC. Simpson: A General Simulation Program for Solid-State NMR Spectroscopy. J Magn Reson. 2000; 147:296–330. [PubMed: 11097821]

44. Bak M, Schultz R, Vosegaard T, Nielsen NC. Specification and Visualization of Anisotropic Interaction Tensors in Polypeptides and Numerical Simulations in Biological Solid-State NMR. J Magn Reson. 2002; 154:28–45. [PubMed: 11820824]

Highlights

R Symmetry-based sequences for ^{1}H CSA recoupling at ultrafast MAS are systematically evaluated.

^{1}H anisotropic / ^{1}H isotropic chemical shift 2D correlation spectra are obtained.

γ-encoded *R* sequences with composite-180 pulses are robust toward RF field inhomogeneity

Precise ^{1}H CSA determination is demonstrated.

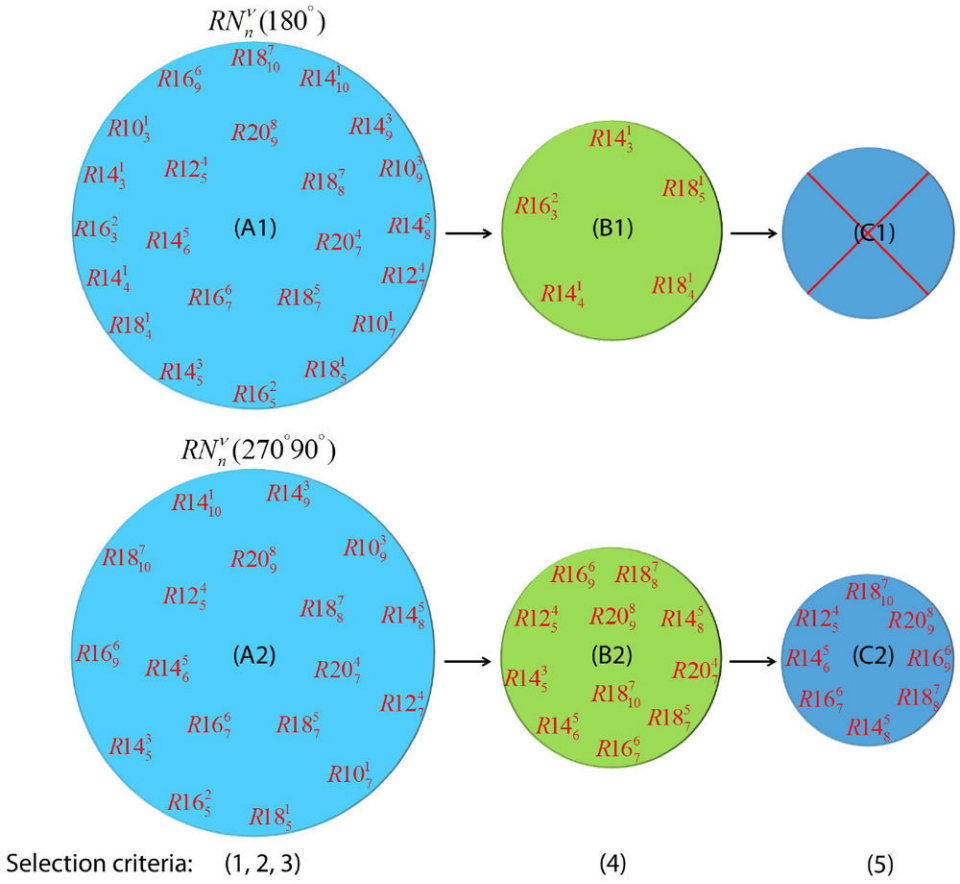

Figure 1.

CSA recoupling sequences based on *R* symmetries with a series of phase-alternating (A1) 180° pulses, and (A2) composite-180° pulses that have RF field amplitude less than 200 kHz at a MAS rate of 70 kHz. (B1, B2) CSA recoupling sequences with a scaling factor $|\kappa_{lm\lambda\mu}| \geq 0.13$ from A1 and A2, respectively. (C1, C2) All listed symmetry-based sequences showed relatively small center peak intensity in the presence of RF field inhomogeneity from numerical simulations using SIMPSON.

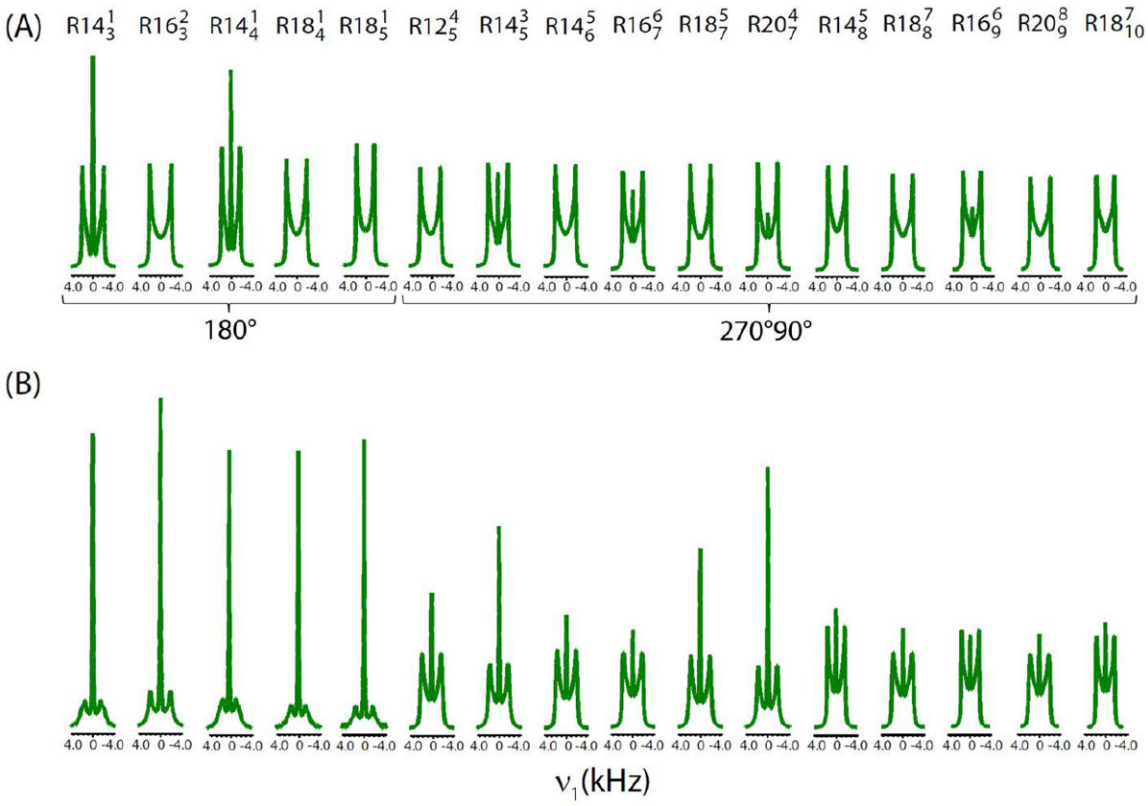

Figure 2.

Recoupled ^{1}H CSA lineshapes generated from SIMPSON simulations using symmetry-based sequences $R14_3^1$, $R16_3^2$, $R14_4^1$, $R18_4^1$ and $R18_5^1$ with a series of phase-alternating 180° pulses and $R12_5^4$, $R14_5^3$, $R14_6^5$, $R16_7^6$, $R18_7^5$, $R20_7^4$, $R14_8^5$, $R18_8^7$, $R16_9^6$, $R20_9^8$ and $R18_{10}^7$ with a series of phase-alternating $270°_0$-$90°_{180}$ composite-180° pulses having a scaling factor $|\kappa_{lm\lambda\mu}| \geq 0.13$ in the absence (A) and presence (B) of RF field inhomogeneity. All simulations were carried out for a single ^{1}H spin at a Larmor frequency of 700 MHz and MAS rate of 70 kHz. Powder averaging was achieved using 678 (α, β) orientations and 26 γ angles with a fixed CSA value of 24 ppm and an asymmetry parameter (η) equals to zero.

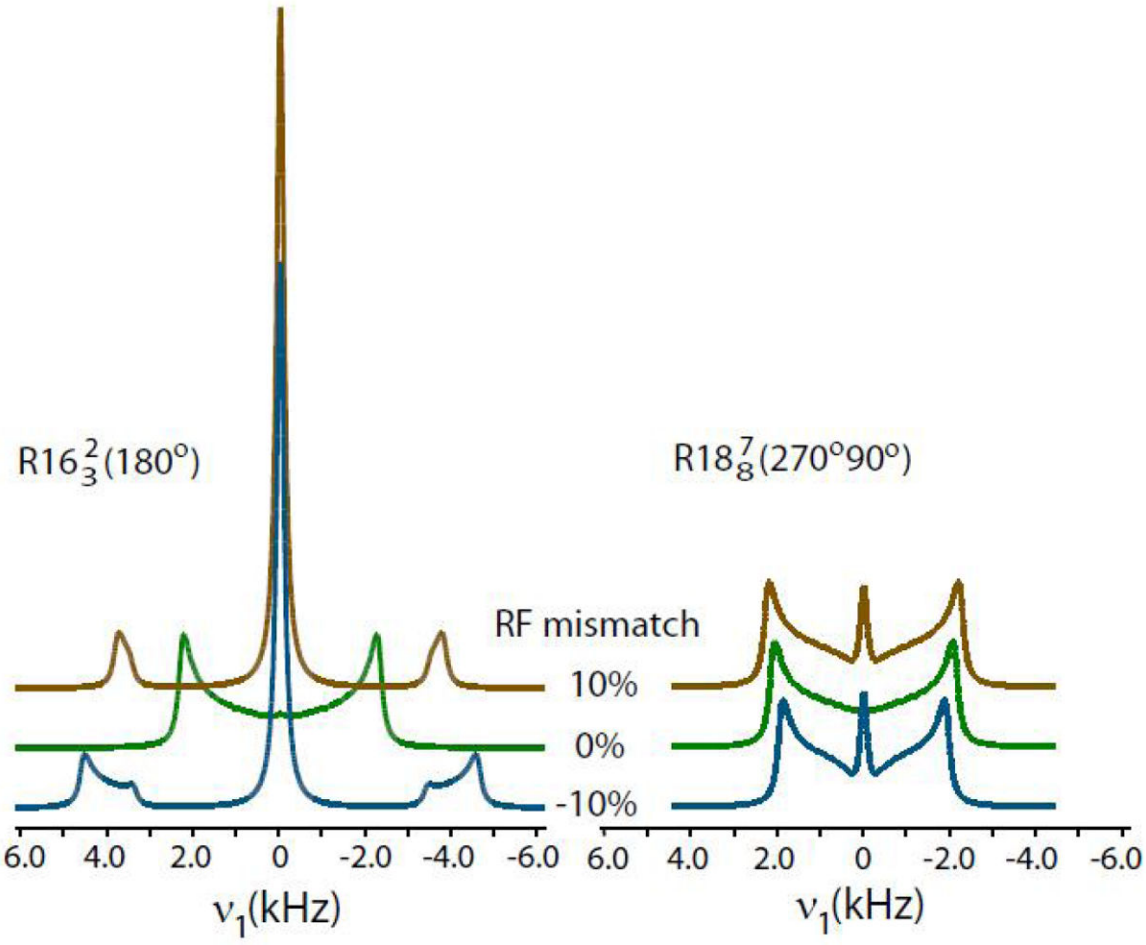

Figure 3.

SIMPSON simulations of recoupled ^{1}H CSA lineshapes as a function of RF amplitude mismatch (±10%) from the theoretical value using symmetry-based sequences $R16_3^2$ employing a series of phase-alternating 180° pulses, and $R18_8^7$ with a series of phase-alternating $270°_0$-$90°_{180}$ composite-180° pulses. All other simulation details are as mentioned in Figure 2 caption.

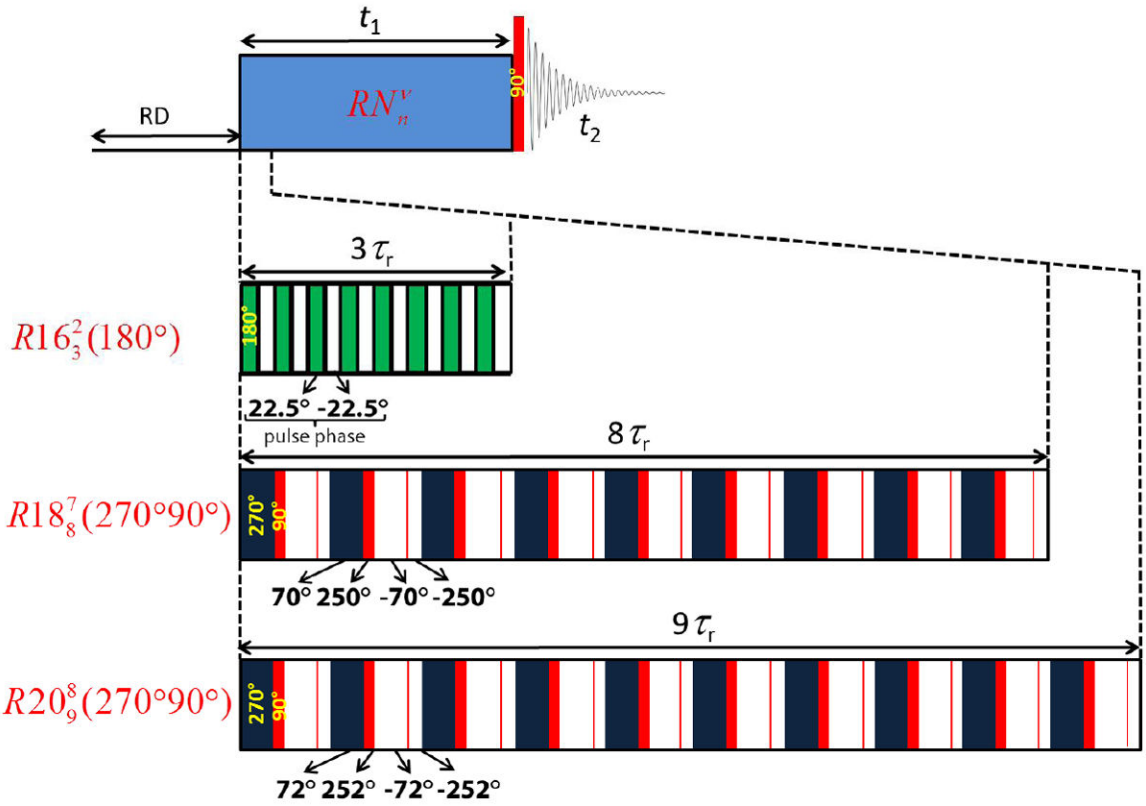

Figure 4.

Symmetry-based pulse sequences $R16_3^2(180°)$, $R18_8^7(270°90°)$ and $R20_9^8(270°90°)$ to record proton-detected 2D ^{1}H/^{1}H anisotropic/isotropic chemical shift correlation spectra at ultrafast MAS frequencies. $R16_3^2(180°)$ is a series of 180° pulses with phases alternating between +22.5 (green rectangle) and -22.5 (unfilled/white rectangle). $R18_8^7(270°90°)$ is a series of (270°, 90°) pulses with phases alternating between (70°, 250°) (depicted as black and red rectangles) and (-70°, 250°) (depicted as unfilled/white rectangles). $R20_9^8(270°, 90°)$ is a series of (270°, 90°) pulses with phases alternating between (72°, 252°) (depicted as black and red rectangles) and (-72°, -252°) (depicted as unfilled/white rectangles). More details can be found in Table 1. After the relaxation delay (RD), the thermal equilibrium longitudinal magnetization is allowed to evolve under the recoupled ^{1}H CSA interaction during the incrementable t_1 period following which a 90° pulse is applied to prepare the magnetization for detection. 2D spectra were collected without the application of homonuclear dipolar decoupling during the detection period t_2.

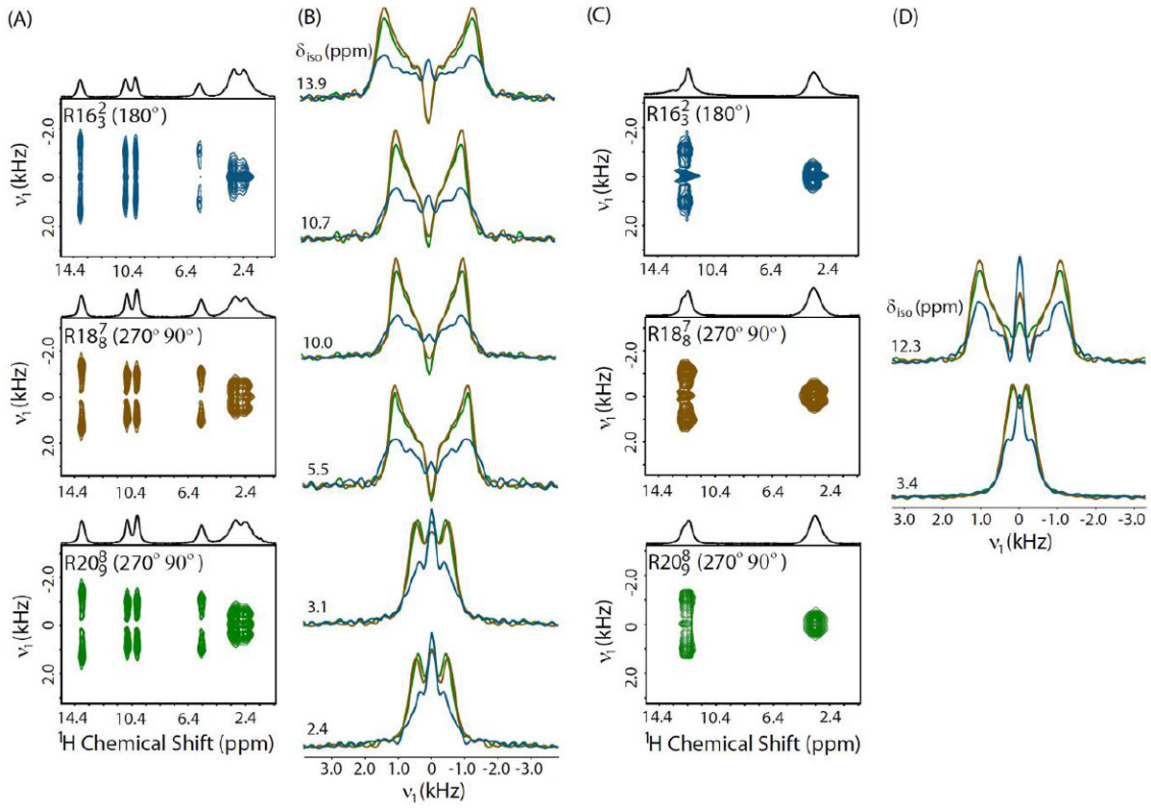

Figure 5.

Two dimensional ^{1}H/^{1}H anisotropic/isotropic chemical shift correlation spectra of citric acid (A) and malonic acid (C) at 70 and 60 kHz MAS, respectively, recorded using symmetry-based $R16_3^2\,(180^\circ)$ (blue), $R18_8^7\,(270^\circ 90^\circ)$ (brown) and $R20_9^8\,(270^\circ 90^\circ)$ (green) pulse sequences from a 700 MHz NMR spectrometer. Recoupled ^{1}H CSA lineshapes obtained from spectral slices parallel to the anisotropic dimension (ν_1) extracted at isotropic ^{1}H chemical shift values in the direct dimension for citric acid (B) and malonic acid (D), respectively.

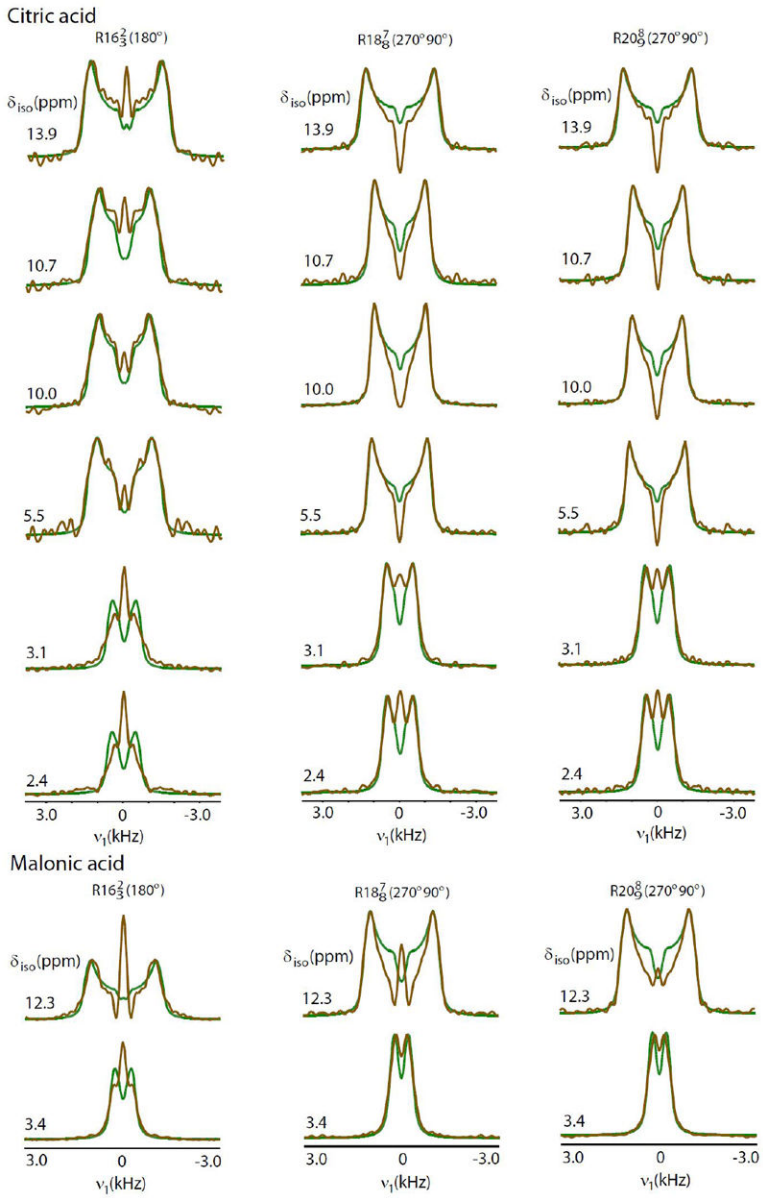

Figure 6.

SIMPSON simulations (green lines) to extract chemical shift parameters from the best fit of experimentally measured spectral slices (brown lines) parallel to anisotropic dimension (ν_1) at isotropic ^{1}H chemical shift values for citric acid and malonic acid under 70 and 60 kHz MAS, respectively, by implementing symmetry-based sequences $R16_3^2\,(180^\circ)$, $R18_8^7\,(270^\circ 90^\circ)$ and $R20_9^8\,(270^\circ 90^\circ)$ at 700 MHz spectrometer.

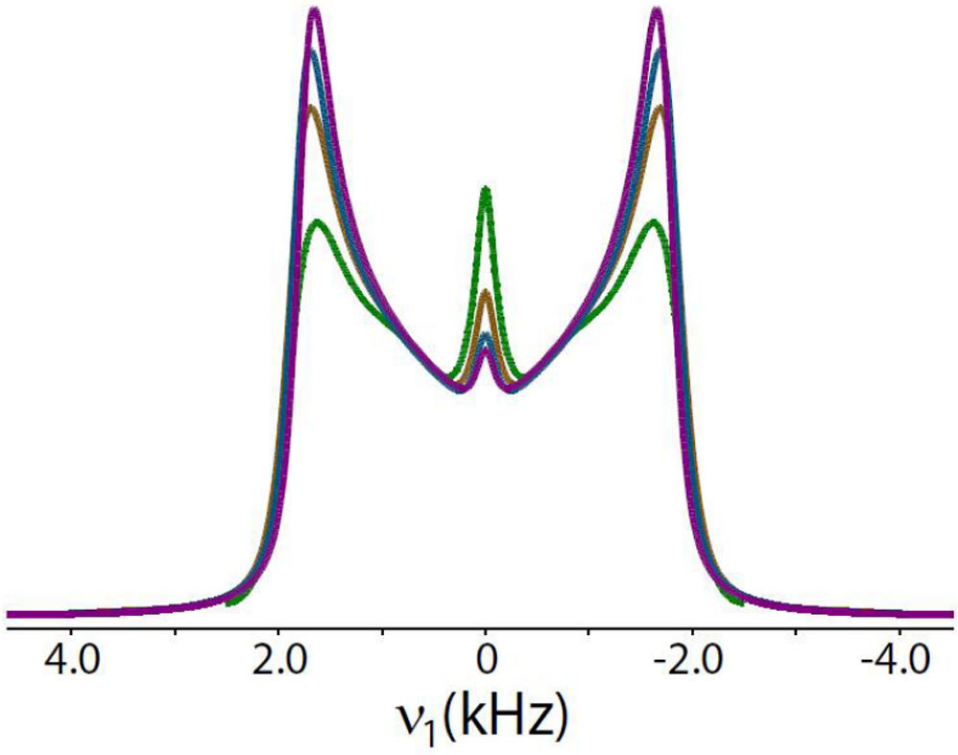

Figure 7.

Recoupled ^{1}H CSA lineshapes of a five spin network representative of −CH_2−CH−CH_2− system generated from SIMPSON simulations using a symmetry-based sequence $R18_8^7\,(270^\circ 90^\circ)$ at MAS rates of 40 kHz (green), 60 kHz (brown), 80 kHz (blue) and 100 kHz (magenta). The initial density operator was taken as a sum of initial z-magnetization associated with each spin while the recoupling efficiency was simulated for the −CH− proton. All simulations were carried out at a ^{1}H Larmor frequency of 600 MHz in the absence of RF field inhomogeneity while powder averaging was achieved using 678 (α, β) orientations and 26 γ angles with a fixed CSA (δ_{ani}) value of 24 ppm and an asymmetry parameter (η) equals to zero.

Table 1

Parameters associated with γ-encoded symmetry-based sequences used in the present study at MAS rates (ν_r) of 70 and 60 kHz for powder samples of citric acid and malonic acid, respectively. The phase shift (φ) associated with pulses in each *R* element is calculated using the relation $\pm \pi\nu/N$ while the corresponding RF field strength is calculated using the equations $N\nu_r/2n$ for $R16_3^2\,(180^\circ)$, and $N\nu_r/n$ for $R18_8^7\,(270^\circ 90^\circ)$ and $R20_9^8\,(270^\circ 90^\circ)$.

Symmetry sequence	*N, n, ν*	*R*	*R'*	R_{φ}	R'_{ϕ}	RF amplitude (kHz)	
						ν_r	
						70kHz	60kHz
$R16_3^2\,(180^\circ)$	16, 3, 2	180_0	180_0	$180_{22.5}$	$180_{-22.5}$	186.7	160.0
$R18_8^7\,(270^\circ 90^\circ)$	18, 8, 7	$270_0 90_{180}$	$270_0 90_{180}$	$270_{70} 90_{250}$	$270_{-70} 90_{-250}$	157.5	135.0
$R20_9^8\,(270^\circ 90^\circ)$	20, 9, 8	$270_0 90_{180}$	$270_0 90_{180}$	$270_{72} 90_{252}$	$270_{-72} 90_{-252}$	155.6	133.3

Table 2

^{1}H CSA parameters obtained from fitting experimentally recoupled powder lineshapes for citric acid and malonic acid using symmetry-based sequences $R16_3^2\,(180^\circ)$, $R18_8^7\,(270^\circ 90^\circ)$ and $R20_9^8\,(270^\circ 90^\circ)$.

	δ_{iso} (ppm)	δ_{ani} (ppm)			η		
Citric acid		$R16_3^2\,(180^\circ)$	$R18_8^7\,(270^\circ 90^\circ)$	$R20_9^8\,(270^\circ 90^\circ)$	$R16_3^2\,(180^\circ)$	$R18_8^7\,(270^\circ 90^\circ)$	$R20_9^8\,(270^\circ 90^\circ)$
-COOH	13.9	16.4	16.6	16.6	0.3	0.2	0.2
-COOH	10.7	12.7	12.5	12.5	0.5	0.3	0.3
-COOH	10.0	12.6	12.5	12.5	0.5	0.2	0.3
-OH	5.5	13.4	13.4	13.4	0.5	0.2	0.2
-CH_2-	3.1	6.0	7.1	6.8	0.6	0.5	0.5
-CH_2-	2.4	6.0	7.1	6.5	0.6	0.5	0.5
Malonic acid							
-COOH	12.3	13.0	13.4	13.4	0.3	0.3	0.3
-CH_2-	3.4	3.8	3.7	3.6	0.6	0.7	0.7